System Simulation of a Differential Radiometer Using Standard RF-Microwave Simulators

J. P. Pascual, B. Aja, M. L. de la Fuente, T. Pomposo and E. Artal

SIMULATION 2005 81: 735
DOI: 10.1177/0037549705062014

System Simulation of a Differential Radiometer Using Standard RF-Microwave Simulators

J. P. Pascual
B. Aja
M. L. de la Fuente
T. Pomposo
E. Artal
Dep. Ing. de Comunicaciones
Universidad de Cantabria
Av. De Los Castros S/N
39005 Santander, Spain
pascualp@unican.es

A complete radiometer simulation framework with special emphasis on high frequencies and switched system performance is proposed. The simulation procedures have been tested on a system configuration used in a branch of the 30-GHz Planck Radiometer, which detects radiation from the cosmic microwave background in a window with 20% relative bandwidth centered at 30 GHz. The goal of the article is not to obtain detailed conclusions about this radiometer in particular but to test the viability of proposed techniques in a realistic context. Basic RF performance of an ideal and a more realistic version of the radiometer is compared. Furthermore, the whole system simulation is implemented in the frequency domain and the time domain, on the same platform that is used to design separate microwave components, introducing realistic parameters for the high-frequency components, such us measured S parameters of the amplifiers and measured current-voltage characteristics of the detectors.

Keywords: Radiometer simulation, envelop transient, harmonic balance, 1/f fluctuations, multiple time scales

1. Introduction

The goal of this work is to establish an environment to develop the most complete and realistic simulation of a differential radiometer on a RF-microwave simulation tool. In particular, a branch of the 30-GHz radiometer of the Planck mission has been used to test the proposed procedures, but the intention is not to obtain detailed conclusions about this radiometer in particular but to test the viability of the proposed techniques with a practical example. The Planck Surveyor is a mission of the European Space Agency (ESA) Science Program [1, 2] to perform astronomical investigations in the sub-millimeter and millimeter wave range. The mission will produce calibrated maps of the whole sky with high sensitivity. The Planck mission will characterize small fluctuations in the cosmic microwave background by mapping its anisotropies. An international consortium of research institutions is responsible for the payload scientific instrument. The Planck Low-Frequency Instrument (LFI) receiver is a form of differential radiometer that minimizes 1/f noise due to gain and noise fluctuations.

The Planck 30-GHz radiometers are based on front-end modules (FEM) with InP HEMT amplifiers cooled at 20 K and back-end modules (BEM) with GaAs HEMT amplifiers at room temperature (300 K). The received "signal" comes from the 2.7 K cosmic microwave background (CMB), which is, therefore, below the level of sensitivity achievable. This signal is compared with a 4 K cold reference load. Possible values of equivalent noise temperature for the cryogenic FEM of the radiometer could be between 9 K and 15 K (above 2.7 K and 4 K). Only after a complex statistical data processing based on repetitive measurements is it possible to extract valuable data from these measurements, but this last point is beyond the scope of this work. The receivers are direct detection radiometers where the signal is first amplified sufficiently and then detected with a diode. This scheme requires stability of the amplification chain. The back-end amplifier behavior, in terms of 1/f noise, is an important issue for good suppression of systematic errors. A block diagram of the Planck

SIMULATION, Vol. 81, Issue 11, November 2005 735-755

DOI: 10.1177/0037549705062014

radiometer is depicted in Figure 1. In this case, there is no down conversion through an intermediate frequency, but when a more complex configuration is required, it could easily be included in the simulations. One input is connected to a reference 4 K load; the other input comes from a feed horn receiving the sky signal. The hybrid couplers act as a divider and a combiner, respectively, in a balanced structure containing two branches with low-noise amplifiers and switching phase shifters (180-degree difference in both states). The output signals in the second hybrid are separated into a sky signal and a reference load signal. The use of hybrids leads to the same noise contribution in both signals. Each time the phase shifter switches, the sky signal and the reference load signal change their position at the second hybrid outputs. The cooled front end is connected by rectangular waveguides to the warm back end, where the signals are amplified, band pass filtered (20% bandwidth centered on 30 GHz), and finally converted to DC by a square law diode detector. Each BEM branch provides an independent set of measurement data subtracting successive measurements of each detector output in different phase states. In such a case, suppression of 1/f noise due to gain fluctuations in the back-end amplifiers and detectors is expected to be optimized.

Analytical expressions summarizing the basic operation of the radiometer are detailed in equations (1) through (4), where the meanings of the parameters correspond to the ones appearing in Figure 1. The output-detected voltages at each of the two branches (O_1 and O_2) in the radiometer can be expressed as (1) and (2), respectively.

$$V_{d1} = G_{DC1} \cdot \alpha_1 \cdot \left| g_{B1} \cdot \left[\frac{1}{\sqrt{2}} \left(\left(\frac{v_s + v_r}{\sqrt{2}} + n_{F1} \right) \cdot g_{F1} \cdot e^{j\Phi_1} + \left(\frac{v_s - v_r}{\sqrt{2}} + n_{F2} \right) \cdot g_{F2} \cdot e^{j\Phi_2} \right) + n_{B1} \right] \right|^2, \tag{1}$$

$$V_{d2} = G_{DC2} \cdot \alpha_2 \cdot \left| g_{B2} \cdot \left[\frac{1}{\sqrt{2}} \left(\left(\frac{v_s + v_r}{\sqrt{2}} + n_{F1} \right) \cdot g_{F1} \cdot e^{j\Phi_1} - \left(\frac{v_s - v_r}{\sqrt{2}} + n_{F2} \right) \cdot g_{F2} \cdot e^{j\Phi_2} \right) + n_{B2} \right] \right|^2, \tag{2}$$

where v_s is the noise voltage at the sky horn, v_r is the noise voltage at the reference load, g_{F1} and g_{F2} are the voltage gains of the two amplifiers in the FEM, and their noise voltage contributions are n_{F1} and n_{F2}. Φ_1 and Φ_2 are the phase values introduced by the phase shifters. The voltage gains in the BEM amplifiers are g_{B1} and g_{B2}, and n_{B1} and n_{B2} are their noise voltage contributions. Detectors are considered to have a perfect square law performance with a constant of proportionality of α_1 and α_2, respectively.

To simplify, both amplifiers in the FEM are supposed to have the same gain, g_F, and each amplifier in the BEM also has the same gain, g_B. The product of voltage gain in the FEM by voltage gain in the BEM is denominated as g.

One phase switch is placed in each FEM branch. It connects the Low Noise Amplifier (LNA) outputs to the output hybrid, and it introduces a phase shift of 180 degrees in the signal in one state in relation to the other. Only one phase switch works, and the other is introduced for symmetry; therefore, the phase Φ_1 will always be 0 degrees. The output voltage detected at one branch is proportional to the noise voltage at the sky horn, v_s, or to the noise voltage at the reference load, v_r, according to (3) and (4), respectively.

Case (a): Φ_1 and Φ_2 equal to 0 degrees:

$$V_{d1}(\phi_2 = 0^\circ) = G_{DC1} \cdot \alpha_1 \cdot \left| g \cdot \left(v_s + \frac{n_{F1} + n_{F2}}{\sqrt{2}} + \frac{n_{B1}}{g_F} \right) \right|^2. \tag{3}$$

Case (b): Φ_1 equal to 0 degrees and Φ_2 equal to 180 degrees:

$$V_{d1}(\phi_2 = 180^\circ) = G_{DC1} \cdot \alpha_1 \cdot \left| g \cdot \left(v_r + \frac{n_{F1} + n_{F2}}{\sqrt{2}} + \frac{n_{B1}}{g_F} \right) \right|^2. \tag{4}$$

With the phase switch active, the output voltage will change between sky and reference load at the two outputs. The signal of interest will be obtained by postprocessing of the output voltage, and the goal is to nullify this signal, which measures differences between the sky and the reference load.

It is desirable that the gain and noise level are stable during a whole cycle of the satellite sweeping the sky; therefore, spin frequency of the satellite (1 rpm) defines the upper bound of the acceptable system knee frequency (around 16 mHz). Analytical studies of the Planck system performance have been done [2, 3], but the objective of this study is to develop for the first time, to our knowledge, a complete simulation of the 30-GHz Planck radiometer with special emphasis on RF-microwave and switched system performance.

Radiometer simulation is a quite difficult task, especially compared to conventional communication system simulation, due to the following:

- Radiometer signals (sky and 4 K reference load in this case) are noise-like, compared with modulated carriers in communication systems.
- Frequencies involved in radiometers cover a wide range, from required f-knee around mHz to microwave noise-like signals (up to tenths of GHz). In the case of communication systems, there is a clear distinction between base-band and band-pass signals. Transient envelope simulation allows this broad range to be handled, once the carriers are specified. In our radiometric problem, there is no such clearly defined carrier, but the center frequency could be chosen. The bandwidth is too wide (6 GHz) to allow enough simulation time to reach the mHz range.

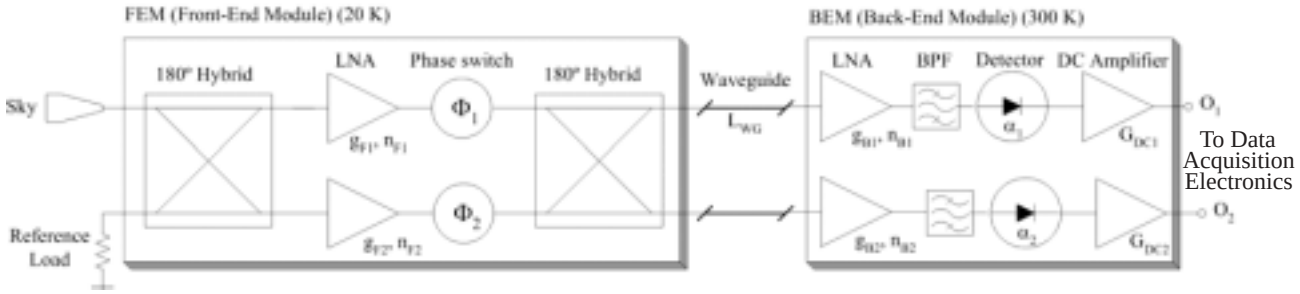

Figure 1. Block diagram of a Planck radiometer

- Mathematical simulation tools [4] using different kinds of transforms—not only Fourier but also wavelets [5] or multiple time scales—are suitable for theoretical analysis, but they are neither prepared nor suitable for introducing parameters of the practical implementation (e.g., S parameters, power compression, current voltage and nonlinear capacitances, etc.).

Small-signal frequency domain simulation is required to test gain, matching, and balance between branches for each state of switching. Large-signal harmonic balance allows evaluation of detector sensitivity in the conversion from RF to DC and gain compression of the amplifiers using single-tone excitation. Both small- and large-signal simulations are fundamental to test microwave performance. But simulation with single tones is different from real operation. The two inputs of the radiometer system are the sky signal (with a power level corresponding to sky temperature of 2.7 K) and the 4 K reference load, both of which are noise-like signals. To test switched differential operation with more realistic noisy input signals, time domain simulation is required. In a pure transient simulation with maximum frequencies involved around 40 GHz (to include filter edges), the time step has to be very small. Simultaneously, a sufficiently long simulating time is required to reach the mHz range. It is not possible to handle both requirements with ordinary computers due to memory restrictions. The use of a transient envelope provides a small improvement. Actually, there is no single carrier because high frequencies lie between 27 GHz and 33 GHz (with 20% of bandwidth around 30 GHz). A first reasonable attempt could be to choose 30 GHz as a carrier, but 6 GHz is too wide a band around the carrier, and the computer memory cannot handle a simulation time, which is long enough to reach the mHz range. These limitations do not mean that transient envelope simulation of the radiometer becomes useless. Accurate quantitative and qualitative results may be obtained in the microwave range, and qualitative results may be achieved for the low-frequency range.

Without a three-time-scale envelope tool available, priority has to be given to simulating one of the frequency bands. This can be done by defining a procedure for frequency scaling. Frequencies involved start almost at DC and reach values around 40 GHz. A linear compression would be a waste of valuable spectrum. Capability limitations of current computers mean that the real-time operation of a system is faster than its virtual simulation on a PC, even for the fastest CPU. According to this, classic frequency scaling divides the maximum frequencies, keeping the lowest unchanged [4]. However, in our approach to the system simulation, the main emphasis is the accurate emulation of the high-frequency parts. Therefore, the scaling method proposed here maintains high frequencies unchanged and only shifts the lower frequencies. This shifting has to be taken into account for the values of DC low-frequency filters. Another possibility is the redefinition of the time base, once simulated data are obtained, to a longer time of simulation with a wider sampling time but with the same number of points.

According to Yarovoy [5], such a system that deals with a signal that instantaneously uses the whole bandwidth can be considered ultra wide band.

Next, in section 2, the models used in the simulations according to the type of simulation (small- and large-signal frequency domain—harmonic balance—and transient and transient envelope) are described. Then, results obtained with the different simulations are discussed for ideal and more realistic cases: small-signal frequency domain in section 3.1, large-signal frequency domain in section 3.2, and time domain in section 4, probing the principles of operation of the radiometer and the reliability and usefulness of the simulations, as well as setting the basis for further improvements in the simulation techniques of such a system.

2. Models for the Simulation

The simulation of the radiometer system has been carried out on a general-purpose RF-microwave circuit and system simulator, including the small- and large-signal frequency domain—harmonic balance—and transient and transient envelope simulators [6].

Simulations on mathematically based platforms rely more on the analytical and functional description of the system. On the other hand, the proposed simulation with the RF-microwave simulator is based more on an accurate

replica of a real system using models for individual elements. Those are, as can be seen in Figure 1, the following: input antenna, reference load, FEM amplifiers, 180-degree hybrids, phase shifters, BEM amplifiers, filters, detectors, and DC amplifiers.

Reliability of results predicted by the simulators depends on adequate phenomena modeling. A brief discussion about the most relevant element models is presented. Matching data of the antenna can be included in the simulation using a procedure proposed in Pascual et al. [7]: the problem arises because antennas are designed with electromagnetic numerical simulation, which provides radiation pattern and input impedance (one-port data), but to simulate RF power flowing through the antenna and entering the amplifiers, converters, and so on, a two-port component is required, providing the same frequency-selectivity and showing the same impedance to the following stages as the original antenna. The RF-microwave simulator employed allows the use of built-in models of amplifiers, where it is possible to include simulated S parameters from the ideal model or real measured S parameters. It is important, when dealing with large gain chains, to include the possibility of the 1-dB compression point as a parameter.

Some of the listed elements of the radiometer (Fig. 1) can be modeled with standard elements of the system library for frequency domain simulations by substituting default parameters with realistic measurement-based values. For transient or transient envelope simulations, special care has to be taken to introduce noise figure and gain-plus-noise fluctuations. The noise figure parameter is normally ignored by transient simulators. Standard amplifier models do not contain any parameter to take into account gain and noise fluctuations. Procedures to overcome these limitations are proposed and verified.

To introduce the amplifier noise figure in transient simulations, a special model is implemented. For detectors, a model similar to the one used in the original RF design is employed. For 180-degree hybrids, a four-port S parameter box is used to introduce nonideal behavior. Voltage-controllable phase switches are implemented with a functional equivalent model. For transient and transient envelope simulations, noise-like signals are generated using noise sources, estimating the value of variance in relation to the noise temperature. Other test signals are single tones (small or large signal) or noisy resistances, which are temperature dependent for frequency domain simulations.

2.1 Noise-Like Signals

The sky signal and reference signal are simulated in transient and transient envelope applications using a noise voltage source. The parameter to specify (*V_Noise*) is the noise spectral density expressed in $V_{rms}/\sqrt{\text{Hz}}$. It can be demonstrated that

$$V\_Noise = \sqrt{K \cdot T \cdot R}\left[\frac{V_{rms}}{\sqrt{\text{Hz}}}\right], \qquad (5)$$

which relates noise spectral density in $V_{rms}/\sqrt{\text{Hz}}$ to noise temperature, where K is the Boltzmann constant (1.38e-23 Joules/Kelvin), T is the noise temperature (K), *V_Noise* is the spectral density in $V_{rms}/\sqrt{\text{Hz}}$, and R is the load resistor in Ohms.

Bandwidth of the simulation is used to evaluate the noise power, according to the specified power spectral density.

2.2 Amplifiers

Amplifiers can be introduced in the RF-microwave simulator mainly in three ways:

- RF amplifier built-in model
- Measured S parameter box
- Gain-controllable amplifier built-in model

The RF amplifier model allows the specification of a constant value for the S parameters. In this case, it is necessary to include input and output filters to define the band (to avoid gain and matching being flat over the whole spectrum). Another possibility is to separately read frequency-dependent S parameters taken from measured data sets. It is also possible to introduce values for the noise figure, 1-dB compression point, and third-order interception point. When defining noise figure in this way, it may not be properly taken into account by transient simulation. This aspect is discussed later.

FEM amplifiers are simulated with the first and the last methods (to include 1/f gain fluctuations in transient simulation). BEM amplifiers are simulated with the first two methods because BEM prototype measurements are available [8]. In particular, a postdetection—DC—amplifier is introduced as a gain-controllable amplifier to include 1/f gain and noise fluctuation.

2.3 Noise Figure and 1/f Noise in Transient Simulation

Noise figure is the most commonly used parameter to specify noise added by an amplifier in RF and microwave terminology, and it is directly related to the noise temperature. Transient analysis of amplifiers does not take into account the noise figure parameter (only considered in frequency domain simulations). A solution adopted to include noise is the addition at the input of the amplifier of a noise source with an estimated value according to the emulated noise figure F (supposedly known). A built-in model of high-impedance adder requiring resistors to fix the matching value is used to perform the addition of noise to the main input. To fix the value of the voltage noise source, it is necessary to know the amplifier-equivalent noise temperature T_e. T_e is the temperature of a source resistor that, when placed at the input of an ideal (noiseless) amplifier, provides at the output the same noise as a real noisy amplifier with 0 K noise resistance at the input. T_e can be obtained as

a function of F, and a relationship between spectral densities in $V_{rms}/\sqrt{\text{Hz}}$ at the input and the amplifier noise figure F can be obtained:

$$V\_Noise = \sqrt{K \cdot T_o \cdot (F-1) \cdot R}\left[\frac{V_{rms}}{\sqrt{\text{Hz}}}\right], \quad (6)$$

where T_o is the reference temperature (290 K), K is the Boltzmann constant (1.38e-23 Joules/Kelvin), F is the noise figure of the amplifier, and R is the impedance of reference in Ohms.

Several simulations were performed to verify the good agreement of the estimated *V_Noise* values.

Thermal noise is included at the input of the FEM amplifier and at the RF section of the BEM.

Gain and temperature fluctuations come from 1/f noise. Both can be simultaneously modeled by applying a noisy signal to the control port of a gain voltage-controlled amplifier with white noise added at the input. Gain-controlling noisy signal is obtained by low-pass filtering of thermal noise. Cut frequency and shape of the low-pass filter fix the speed of gain fluctuation and, therefore, the knee frequency. The level of noisy signal is arbitrarily adjusted to provide sufficient evidence of the effect. Low-frequency noise modeling of specific devices is beyond the scope of this work, but it is compatible with it for further development.

The controlling signal is the key to ensure proper and realistic gain fluctuation. The following is a brief discussion about this. An example of the scheme to simulate the generation of such a white plus 1/f noisy signal is given in Figure 2.

The adder model has infinite impedance at the input; therefore, resistors are placed to provide expected loading to the noise voltage sources.

Three different spectra appear in these simulations. In Figure 3, spectral densities, including white and 1/f noise, are represented in dBm/Hz:

- White noise (Fig. 3a)
- 1/f noise ("spectrum_flicker") (Fig. 3b)
- White plus 1/f noise ("spectrum_white+flicker") (Fig. 3c)

In Figure 3c, the knee frequency ($f_{K_{nee}}$) can be graphically estimated by the intersection of two lines, one horizontal and the other with a slope of –10 dB per decade (in fact, $f_{K_{nee}}$ corresponds to the point 3 dB higher). In the radiometer, real $f_{K_{nee}}$ after processing can be around mHz, but the simulator cannot simultaneously handle such a low frequency with millimeter wave noise. In this case, to preserve high-frequency characterization, frequency scaling has been done upwards.

The procedure described for generating a noisy signal allows the direct control of $f_{K_{nee}}$, but it is inconvenient when used to apply to the gain control port of an amplifier: it modifies the noise figure of the amplifier by an amount that depends on the level of input signal due to the addition of thermal (white) noise in the control voltage. Therefore, a version without white noise added at the control voltage was preferred.

The estimation of the radiometer output signal $f_{K_{nee}}$ is done by numerical integration across the output bandwidth of noise power with 1/f sources "on" to compare with 1/f sources "off." This procedure is more accurate than graphical methods. A discussion about this is presented later.

Two sources of 1/f fluctuation will be included in the system:

1. In the FEM, 1/f noise is included in the RF gain chain.
2. In the BEM, 1/f noise is included in the DC amplification, after the detector.

2.3.1 FEM 1/f Noise

A critical task is to include 1/f noise in the FEM gain to check its cancellation during the switched operation of the balanced radiometer. The proposed method to introduce 1/f noise in the gain of the amplifier also represents 1/f temperature fluctuations, modeling phenomena in a complete approach (a more complex model structure could be implemented to ensure full noncorrelation between gain and temperature fluctuations).

The described procedure was applied to a gain-controllable amplifier, operating in the RF band, to introduce 1/f gain fluctuations in the FEM. Special care was taken with impedances because the built-in gain-controllable amplifier seems to be designed more for low frequencies and high impedances; therefore, some matching resistances were added to allow ideal or realistic input and output matching. Another aspect to take into account is the introduction of added thermal noise at the input. At the input of the FEM gain-controllable amplifier, an adder is placed to combine the main input with the thermal noise source. As in the BEM, resistors are placed at each input of the adder to provide the input matching level and the 50-Ohm load of the voltage noise source. Ideal filters are placed before and after the amplifier to define the band.

1/f gain fluctuations are introduced in the gain control port of the amplifier as a voltage noise source and low-pass filtered to fix the knee frequency. Gain of the amplifier is a combination of a constant value plus the 1/f fluctuating signal. In a realistic approach, values are fixed to provided 34-dB gain and input and output matching corresponding to –10 dB. A scheme of the amplifier model is depicted in Figure 4.

Some tests were performed on the model to verify its behavior. Scattering parameters were obtained to validate proper small-signal RF operation (see gain and matching in Fig. 5). In a transient envelope analysis, a single tone at 30 GHz plus white noise was applied at the input of the amplifier, and the output spectrum was plotted with and without 1/f gain fluctuation applied. Depending on the

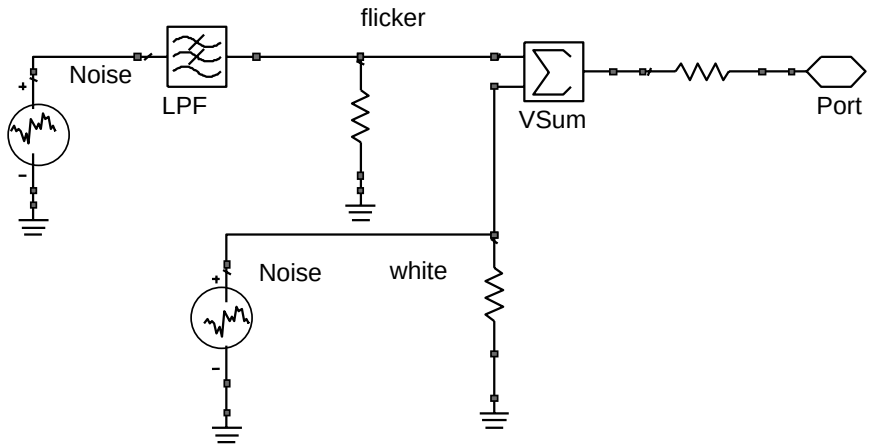

Figure 2. Generation of white plus 1/f noise

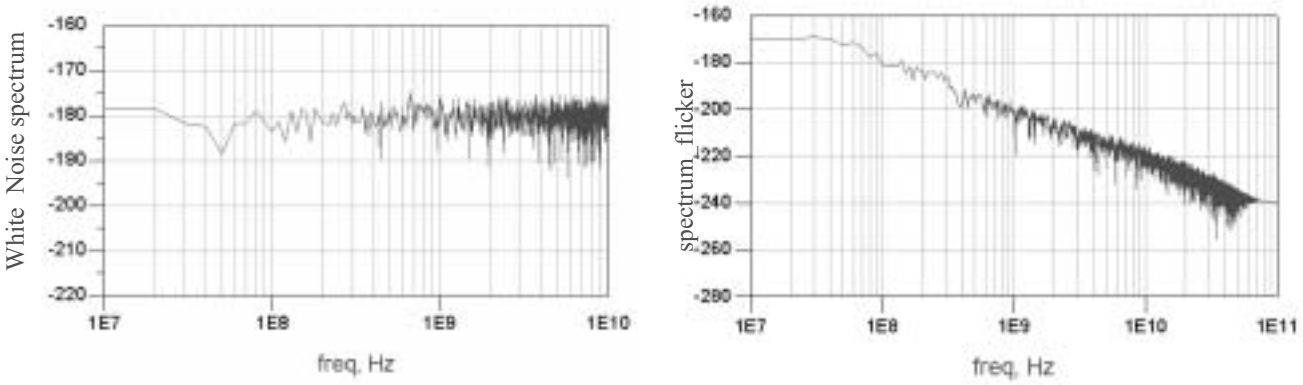

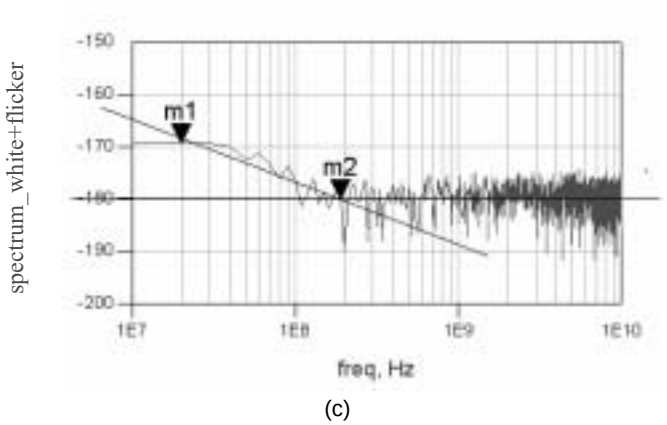

Figure 3. (a) White noise spectrum. (b) 1/f noise. (c) White + 1/f noise.

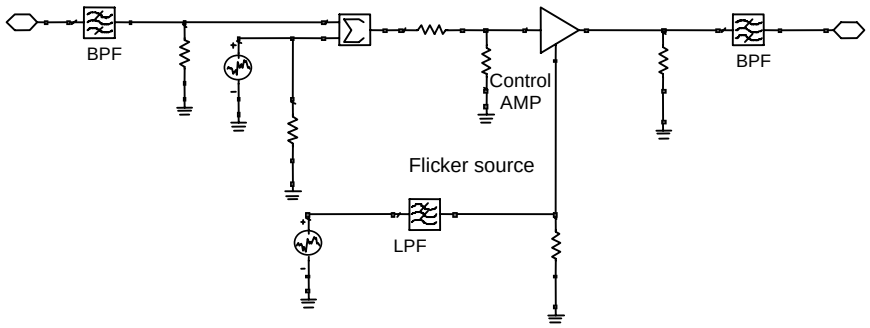

Figure 4. Amplifier model for the front-end module (FEM)

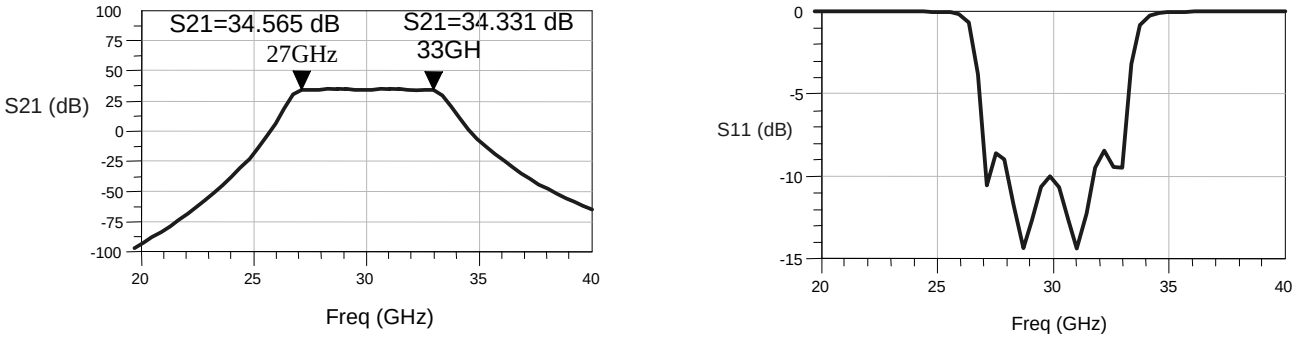

Figure 5. Scattering parameters (gain and input matching) of the front-end module (FEM) amplifier model

filter and noise amplitude in the 1/f block, the shape of the output spectrum can vary (Fig. 6 shows control signals and the output spectrum for different cases obtained by transient envelope to compare and appreciate the effect).

Other elements in the FEM such as phase shifters can introduce 1/f fluctuation, but this first approach is to focus on the viability of considering 1/f amplifier gain fluctuations [9] without other sources.

2.3.2 BEM 1/f Noise

The same model as the FEM could be used in the BEM. Moreover, gain fluctuation in the DC amplifiers, after the detector, is also taken into account. RF models and measurements of the BEM were locally available [8].

The DC amplifier after the detector is implemented with a gain-controlled block, and it is used to include 1/f noise from the BEM in the simulation of the system. Its gain (nominally 200) is controlled by a noisy signal. A simple test is simulated to obtain a fluctuating gain: a DC 1-mV signal is applied at the input of the amplifier, obtaining an amplified fluctuating signal at the output. In Figure 7, the following results are shown, proving that gain fluctuations in the BEM affect the output signal:

- DC input signal
- Noisy signal that controls DC amplifier gain ("V_white+flicker")
- Voltage gain of the amplifier
- Output voltage of the DC amplifier ("V_{Out}")

Other elements in the BEM, such as the detector, could also introduce 1/f fluctuations, but as in the case of phase shifters, in this first approach, it has not been included.

2.4 180-Degree Hybrids

The 180-degree hybrids provide balance operation to the radiometer. Built-in models were not considered adequate for our purpose, and four-port S parameters boxes were preferred. Two different sets of values were used, depending on the kind of performance desired: ideal or realistic performance (with poorer isolation and matching).

2.5 Detectors

Detectors were modeled using an input filter loaded with a resistor and a series diode, terminated with a capacitor plus an RC filter on the DC side. Values of the elements were chosen to simultaneously reproduce realistic values of the following:

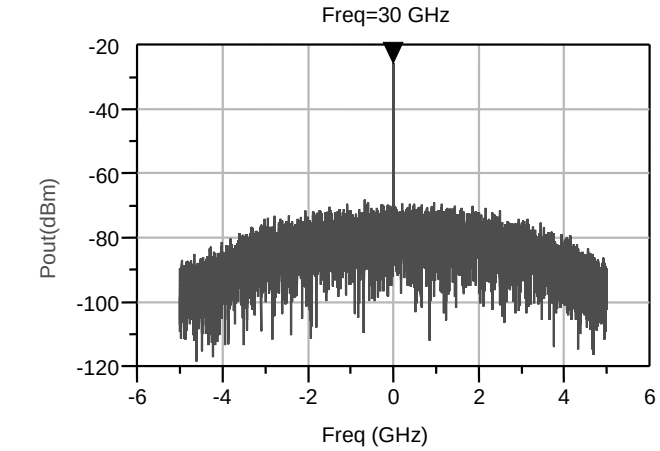

Pin=-60 dBm @ 30 GHz

(a)

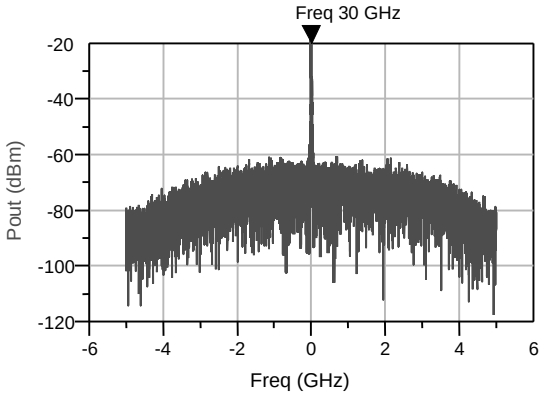

Pin=-60 dBm @ 30 GHz

(b)

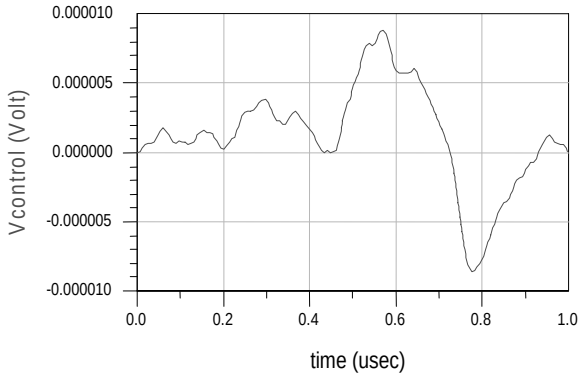

(c)

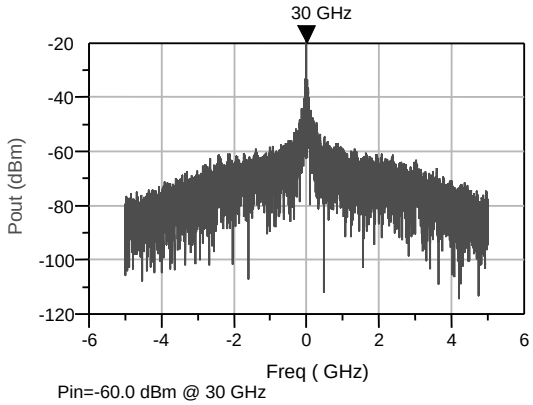

Pin=-60.0 dBm @ 30 GHz

(d)

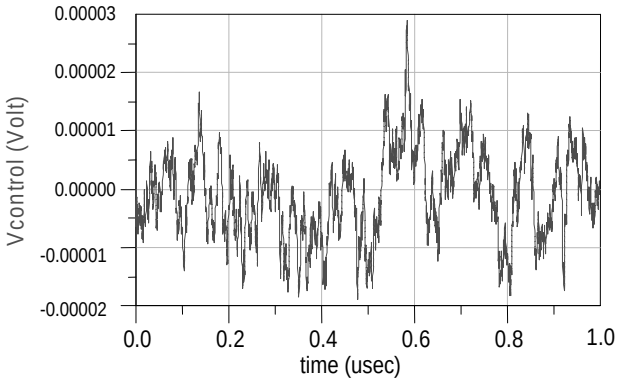

(e)

Figure 6. Output spectra of the front-end module (FEM) amplifier model: (a) no gain fluctuation, (b) slow gain fluctuation, and (c) gain control voltage causing slow gain fluctuation. (d) Output spectrum with fast gain fluctuation and (e) gain control signal causing fast gain fluctuation. Notice that in (a), (b), and (d), frequencies are relative to the carrier.

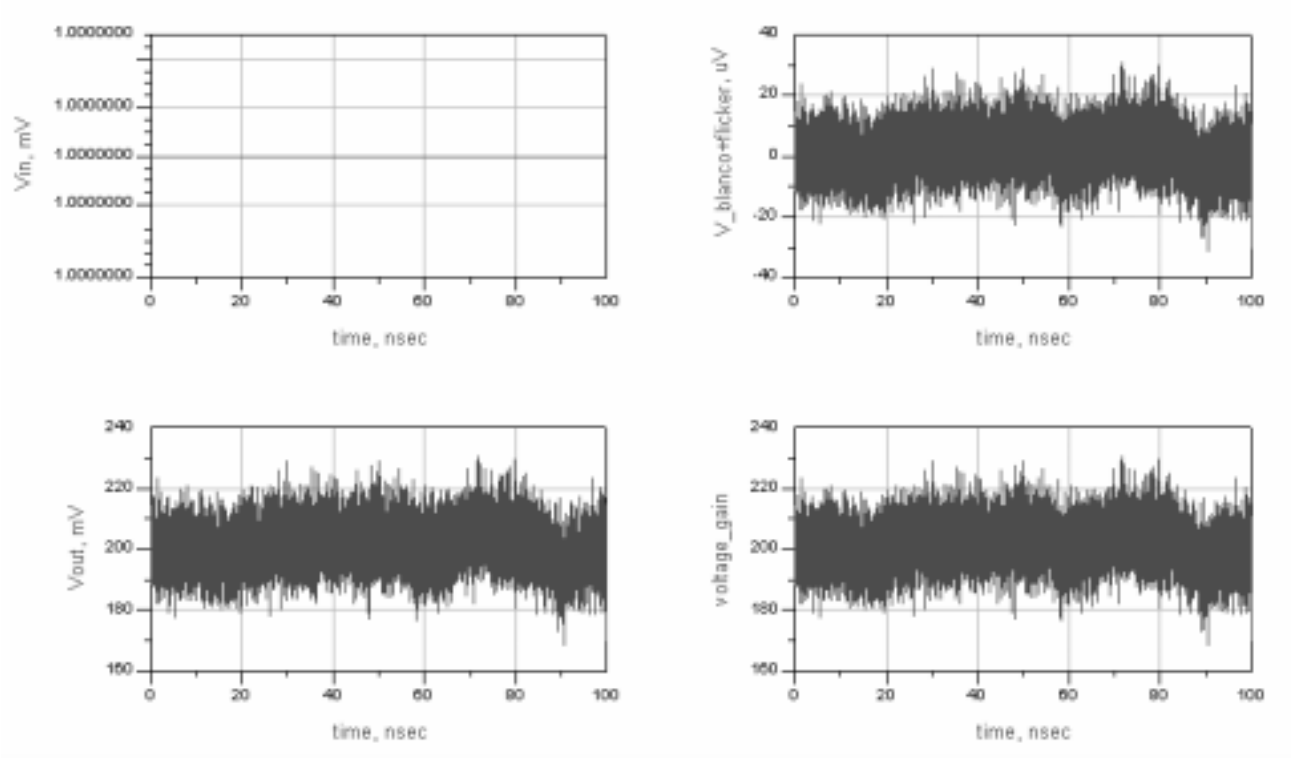

Figure 7. Simulation of the amplifier controlled by a noisy signal: DC input signal (top left), control signal (top right), output signal (bottom left), and voltage gain (bottom right)

- Input matching
- Sensitivity (mV/mW)
- 1-dB compression

The complete and detailed simulated design can be used. Input matching of the detector is shown in Figure 8. Conversion from RF to DC at 30-GHz sweeping input power is plotted in Figure 9.

It is possible to use directly measured RF-to-DC conversion values by means of an element called the frequency-defined device (FDD) [6], especially conceived to enable behavioral modeling.

2.6 Phase Switches

Two possibilities were used: the first one consists of phase shift elements combined in a two-path switched structure. The second is a mathematical block that multiplies the input signal by a pulsed signal (switching between –1 and +1). Both are suitable for frequency or time simulations, but the former is more appropriate for introducing a phase mismatch between branches.

A scheme of both topologies is depicted in Figure 10.

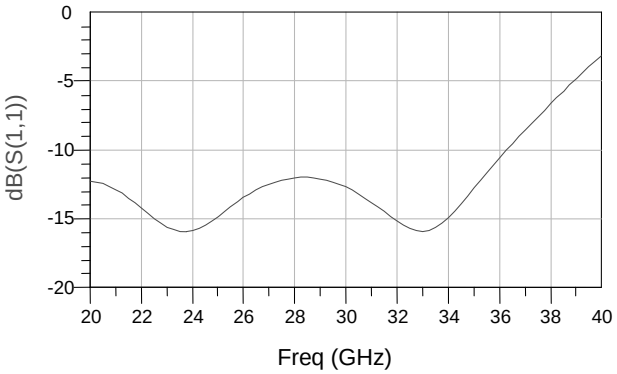

Figure 8. Input matching of the detector

2.7 Single-Branch Self-Comparison Implementation

One of the methods to combine the outputs of the radiometer is to integrate the difference of each branch compared to itself, but in a different phase shift state. This is implemented using an element that introduces a time delay

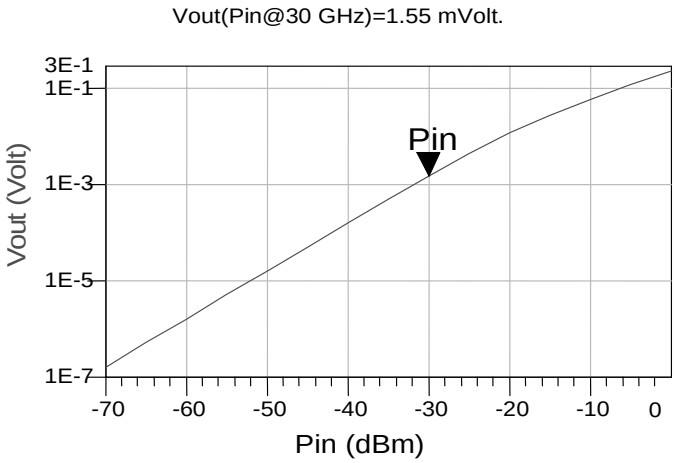

Figure 9. DC output versus input power at 30 GHz

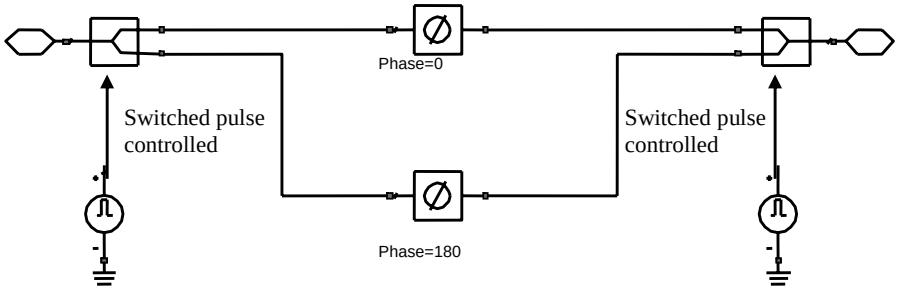

(a)

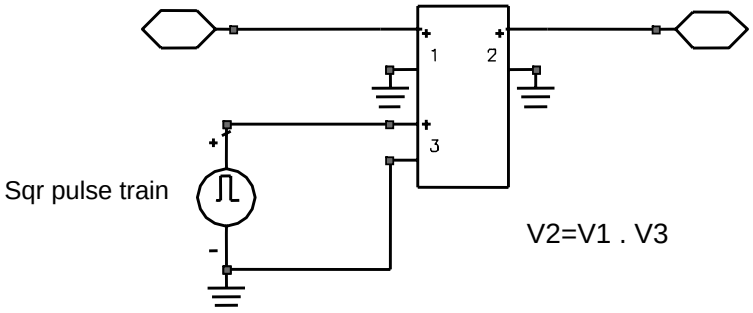

(b)

Figure 10. Models for phase switch: (a) two-path switched structure and (b) multiplier structure

and the differential inputs of an Op-Amp. The time delay built-in block was not found adequate, and the delay introduced by the voltage-controlled voltage source was preferred. Time delay is fixed at half of the period of the phase-switching signal to ensure that proper comparison is done. Data obtained from simulations can be processed in the same environment or stored in ASCII files and processed in other software applications. Even time scales can be modified (redefined) during processing to make results closer to real time scales.

3. Frequency Domain Simulation

Frequency domain simulation is the basic tool to test proper performance of the system. Considering static cases corresponding to fixed phase shifts (not switched), RF gain, matching, isolation, and effective bandwidth can be checked by using small-signal simulation. Moreover, considering the RF-to-DC conversion of the detector, input matching, sensitivity, and linearity should be verified. For that, a large-signal (harmonic balance) simulation is required.

3.1 Small-Signal Frequency Domain Simulation

3.1.1 Ideal and Realistic Radiometer

The ideal radiometer has ideal hybrids and ideal amplifiers perfectly matched and an exact 180-degree phase shift. The realistic radiometer has hybrids with finite isolation, phase shift close to 180 degrees but not exactly equal, and amplifiers with limited matching. More realistic simulations have been done with available measured scattering and noise parameters of the BEM (see Fig. 11 for RF gain of the radiometer with measured data of the BEM for fixed phase shift).

3.1.2 Isolation

It is in this parameter that the difference between ideal and realistic performance shows itself more clearly. S parameters are referred to the following numbering: port 1 sky, port 2 reference, port 3 output branch #1 (before detector), and port 4 output branch #2 (before detector). Phase switches have fixed values (0 or 180) that define a phase state.

Figure 11 shows S_{31} for realistic elements. For an ideal radiometer, values around –260 dB (almost "perfect" isolation) are obtained. Notice the great impact in realistic isolation, with "undesired" transmission only around 45 dB below "desired" transmission. Nevertheless, these values can still be considered acceptable.

Maximum isolation is obtained with phase shift exactly equal to 180 degrees. Phase shift deviations cause a degradation of isolation (see Fig. 12 for transmission to the isolated port vs. phase of branch #2 phase shifter at 30 GHz for realistic parameters).

3.1.3 Noise Figure

It is possible to simulate, by an RF linear analysis (with the system terminated before the detector), the noise figure corresponding to each output. Placing port #1 in the sky input, it can be verified that noise figure increases drastically at each output when phase switch does not correspond to that path: with phase switch in branch #1 at 0 degrees and phase switch in branch #2 at 180 degrees, sky signal must flow mainly to the output of branch #1 and only a residual part to the output of branch #2. This means that the noise seen from branch #1 output is the minimum (e.g., around 0.13 dB, corresponding to 9 K), and noise seen from branch #2 output is quite high (above 30 dB) when the signal comes from the sky port. With phase switch in branch #2 at 0 degrees, the situation is the inverse.

A critical aspect is to determine the influence of FEM gain on system noise. An analysis is done, sweeping the gain of the FEM amplifiers from 25 to 35 dB, supposing they have a constant noise figure (0.13 dB or 9 K), to check the increase of noise contribution from BEM (a reference nominal value of 3.36 dB was taken). This simulation is done with the BEM modeled by library gain blocks or with real measurements of S parameters and noise parameters (the latter corresponds to Fig. 13). As gain is lower than nominal (34 dB), T_e increases in some frequencies around 3 or 4K, up to 14 K when using measured BEM data.

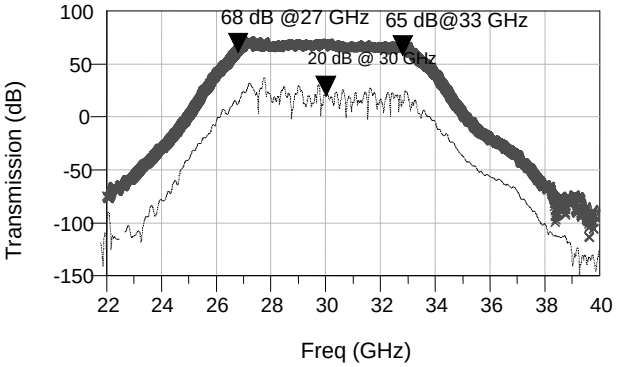

Figure 11. RF transmission gain (x) and transmission to the isolated port (. . .) of the radiometer, simulated by combining the modeled front-end module (FEM) with blocks of partial measurements of the back-end module (BEM). For an ideal radiometer, values of transmission to the isolated port around –260 dB without practical meaning are obtained.

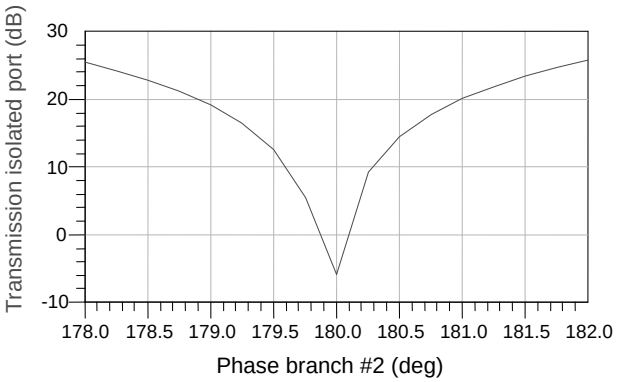

Figure 12. Transmission to the isolated port at 30 GHz versus phase of branch #2 phase shifter for a realistic radiometer

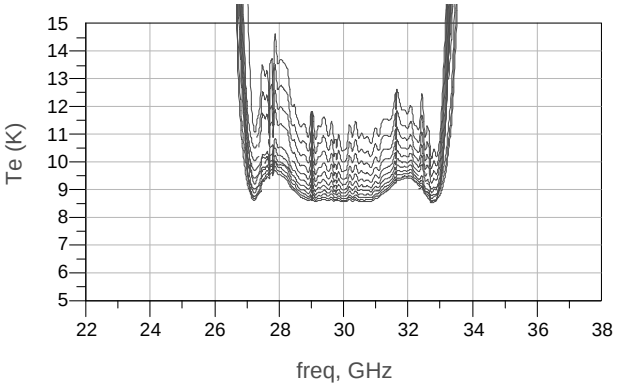

Figure 13. Noise figure variation when front-end module (FEM) gain is swept from 25 to 35 dB. Back-end module (BEM) is represented with real measurements of noise and S parameters.

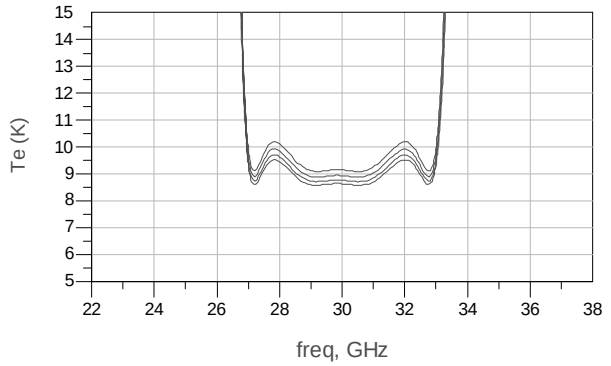

Figure 14. Noise temperature variation when back-end module (BEM) noise figure is swept from 3 to 6 dB

Another approach to the problem is to sweep BEM noise from 3 to 6 dB for fixed FEM gain and noise. This is done in Figure 14. As can be seen, when FEM gain has the nominal value, a dramatic increase in BEM noise with respect to the nominal value has limited impact on total noise temperature (around 1 K in the worst case).

3.1.4 Effective Bandwidth

One of the most significant figures of merit of the radiometer is the effective bandwidth [10], defined by

$$BW_{eff} = \frac{\left[\int_0^\infty G(f)df\right]^2}{\int_0^\infty [G(f)]^2 df}, \qquad (7)$$

where $G(f)$ is the RF power gain. The goal is to have a 20% bandwidth, centered on 30 GHz. The influence of different 3-dB bandwidths in FEM and BEM and the misalignment between FEM and BEM center frequencies have been simulated. As can be seen in Figure 15, an increase in the FEM –3-dB bandwidth does not necessarily mean an increase in effective bandwidth defined by (3), depending on the BEM –3-dB bandwidth. The difference between –3 dB and effective bandwidth should be kept in mind. Moreover, the evaluation of the effective bandwidth of a cascade of two stages depends on the frequency dependence of each stage and the whole cascade. This means that normally, the whole cascade should have lower effective bandwidth than each stage, but it could be also wider if there is some gain compensation between both stages.

A deviation in alignment between FEM and BEM center frequencies causes a decrease in the effective bandwidth (see Fig. 16).

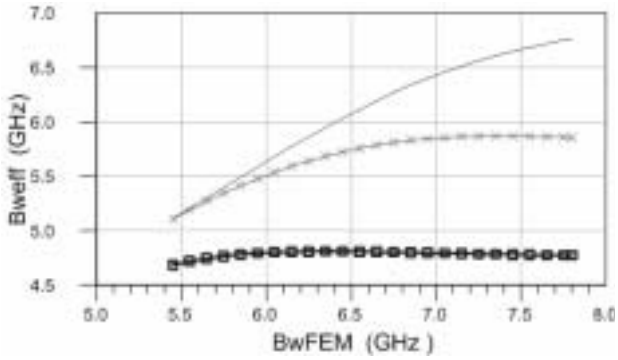

Figure 15. Effect of variation of the –3-dB front-end module (FEM) bandwidth in the total effective bandwidth with three different –3-dB bandwidths of the back-end module (BEM) (5 GHz, squares; 6 GHz, x; 7 GHz, line)

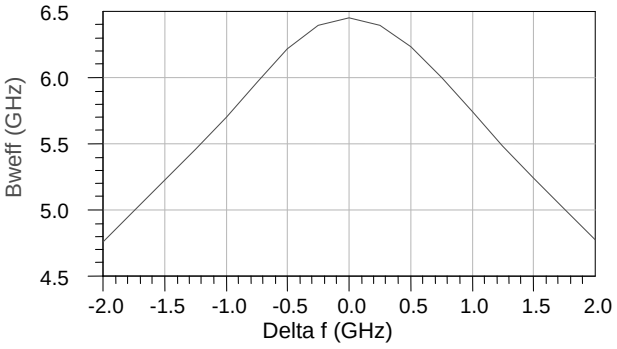

Figure 16. Effective bandwidth with different values of misalignment in front-end module (FEM) and back-end module (BEM) center frequency

The other figure of merit is sensitivity [10], given by the following expression:

$$\frac{\Delta T}{T_{sys}} = \frac{1}{\sqrt{BW_{eff}\tau}}, \quad (8)$$

where BW_{eff} is the RF effective bandwidth before detection defined in (7), and τ is the time constant of the postdetection filter. ΔT is the minimum detectable temperature variation, and T_{sys} is the noise temperature of the system. Small-signal simulations combined with these well-known formulas allow one to obtain relevant conclusions about radiometer performance. In Figure 17, these parameters are combined based on measured prototypes showing that a decrease in sensitivity can be achieved by widening the BEM effective bandwidth, even with an increase of equivalent noise temperature (T_{sys}).

Different simulations were done to evaluate the contributions to the global noise temperature and BW_{eff} of each part (FEM and BEM), showing a major influence of FEM noise and limited influence of BEM BW_{eff}.

3.2 Large-Signal Frequency Domain Simulation

3.2.1 Detection Performance and Linearity

Sky and reference signals have low power levels; however, due to the large gain from the input of the FEM to the output of the BEM and the limited power range of all the elements, particularly the detector, it is important to make a budget analysis of the whole gain chain to avoid saturation of the detector or the DC postprocessing circuitry.

Harmonic balance analysis requires a tone with power level set to the same value as the corresponding highest noisy signal (the 4 K reference in a bandwidth of several GHz, which corresponds to –94.8 dBm). The frequency is swept across the band to obtain the DC levels at the output of the detector. Another possibility is to analyze the whole system, introducing a single tone in the center frequency and sweeping the power. As the problem of saturation arises especially in the BEM, comparisons between model and measurement of the frequency versus DC response with a level of –60 dBm (–94 dBm + 34dB = –60 dBm) injected at the input of the BEM, can be made. Based on measurements, an output –1-dB compression point of –10 dBm was considered for the RF gain block of the BEM (RF amplifiers only, detector not included). Simulations of the complete BEM showed that the detector input compression point causes a slight deviation from the ideal linear response, moving the compression point of the complete BEM (RF and detector) backwards, as has been verified with measurements of a BEM prototype (see Fig. 18).

Simulations and measurements of the BEM RF-to-DC response are shown in Figures 19 and 20 for a –60-dBm single tone. Measured ripple was smaller than expected from simulations using partial measured S parameters due to the effect of all the interconnections present in the complete BEM.

RF-to-DC response was simulated for the complete radiometer, using models from the library (Fig. 21).

With the swept single-tone test, all the power is concentrated in a fixed frequency. DC output in a realistic case (input power spread across the entire band) can be estimated averaging single-tone response.

4. Time Domain Simulation

4.1 Transient and Transient Envelope

Transient simulation is considered to be the closest to "the true behavior" of circuits and systems. Transient simulation of the radiometer has the highest computer cost. A portion of irrelevant bandwidth between a few MHz and ~25 GHz, consuming valuable memory, is analyzed. Therefore, unless transient simulations are also performed, it is preferable to use transient envelope simulations. Irrelevant bandwidth is avoided this way, and lower frequencies are reached, leaving memory available for longer simulations but not long enough to decrease the simulated knee frequencies to real values. Transient envelope [11] is based on the expression of circuit/system signals in terms of a Fourier series with time-varying phasors of limited bandwidth (9).

$$x(t) = \sum_K X_K(t) e^{j\omega_K t}. \quad (9)$$

This simulation tool is especially well suited for modulated signals, startup of oscillators, and so on. In all cases, there are one or several high-frequency carriers (ω_K) and one or several time-varying low-frequency envelopes ($X_K(t)$). The high-frequency components are analyzed with harmonic balance, providing results in the frequency domain, and the envelope phasors are analyzed in the time domain. Compared to conventional transient simulation, the saving in time steps is clear because the sampling rate is fixed by the low-frequency envelope, not by the high frequencies. In the case of the millimeter wave radiometer under study, there are two "virtual" carriers: 0 Hz and 30 GHz and a noisy wide-band modulating envelope. As was explained at the end of section 1, due to the high bandwidth (over 20%), this application of transient envelope becomes a limit case because it forces a still high sampling rate, which limits the maximum time of simulation and therefore the minimum frequency. However, useful data are obtained from simulations and can be processed in the same simulator or stored and processed in other applications that allow the modification of time scales to make results closer to real time scales (see example of time frequency scales in Fig. 22).

The output bandwidth must be below the transient envelope bandwidth (proportional to $1/\Delta t$) and above the knee frequency range to allow a proper representation of the spectrum.

Models for transient simulation are equally suitable for transient envelope simulation, but frequency domain

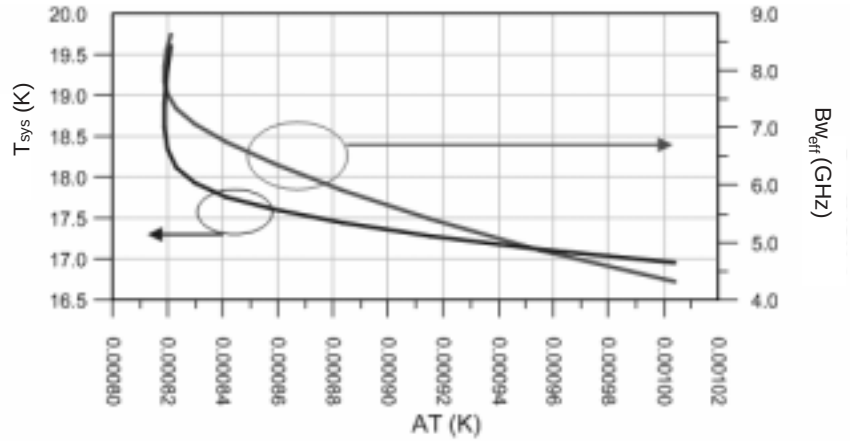

Figure 17. ΔT (sensitivity (K)) versus effective bandwidth BW_{eff} (GHz) of the back-end module (BEM) and equivalent thermal noise temperature T_{sys} (K)

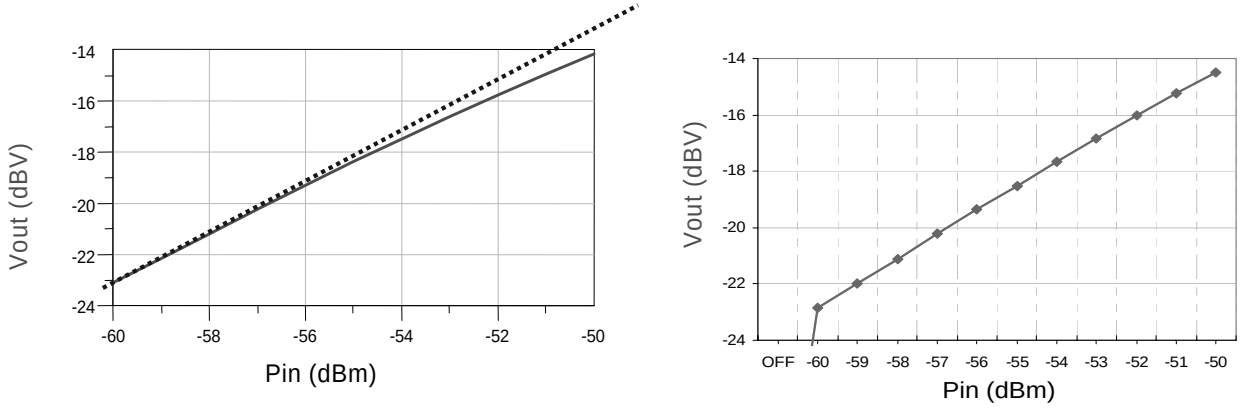

Figure 18. RF-to-DC response of the back-end module (BEM) for a 30-GHz tone that is (a) simulated (continuous line) and superimposed with the ideal linear response (dashed line) and (b) measured.

models are especially well suited for the latter. The only aspect that must be adjusted moving from transient to transient envelope is the shape of the low-pass filters in the 1/f noise generation and in the output of the system (after detection).

Accordingly, the coupling between low-frequency effects and mm-wave effects would be inherently provided by the simulation, showing an improvement compared to separate analysis for RF parts and base-band equivalent.

There are different possibilities to combine the outputs of the radiometer, but the final goal is the same—to make a comparison between sky and reference signal by canceling the difference with a correction factor (usually designated r), which contains the information. The expression of the gain modulation factor is given by

$$r = \frac{T_{sky} + T_n}{T_{load} + T_n}, \tag{10}$$

where T_{sky} is the sky noise temperature, T_{load} is the reference load temperature, and T_n is the system noise temperature.

The r factor will be adjusted periodically; therefore, stability of the system is required.

The signal present at each of the two physical output connectors can be proportional to T_{sky} or T_{ref}, depending on the phase switch state. There are, at least, three possibilities to apply r factor corrections: it is possible to compare both outputs in the same phase switch state, only one output in consecutive phase switch states and even to

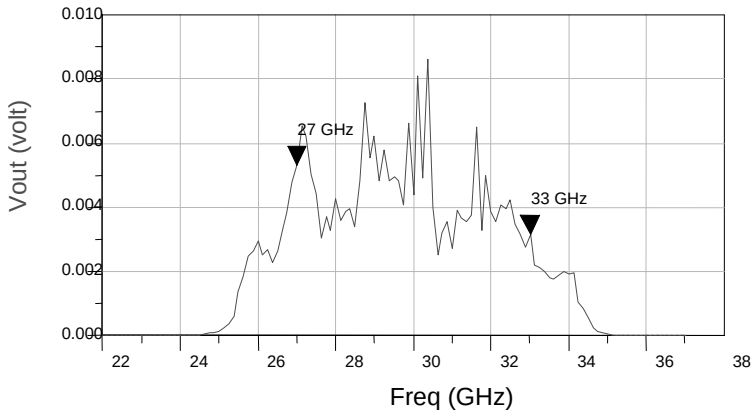

Figure 19. Simulated DC response in band of a measured S parameter–based back-end module (BEM) to a –60-dBm tone

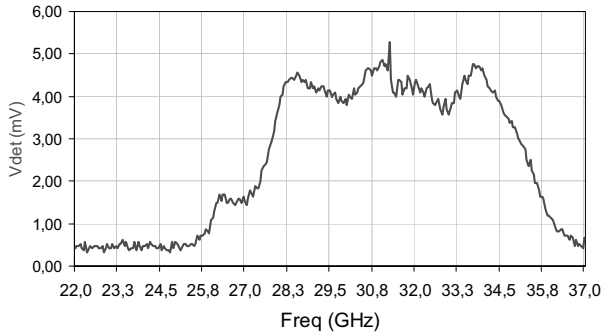

Figure 20. Measured DC response in band of a back-end module (BEM) prototype to a –60-dBm tone

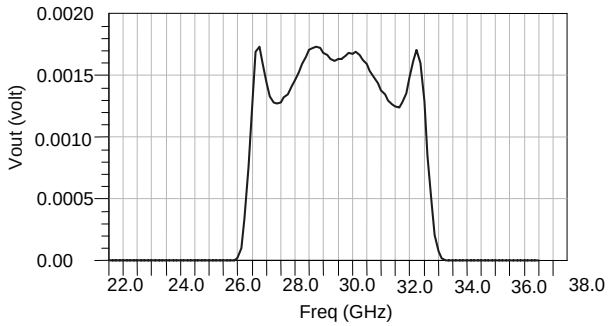

Figure 21. Simulated DC response in band of a system model-based radiometer (front-end module [FEM] + back-end module [BEM]) to a –94.8-dBm tone

take a difference between both channels, but taking in each channel differences of consecutive phase switch states. The third possibility means that there is a difference between two channel magnitudes: the differentiation of consecutive phase switch states in one channel minus the same magnitude in the other channel.

In these simulations, output signal of the radiometer has been analyzed in switched operation. Two kinds of spectra have been obtained: a raw spectrum and a processed spectrum. In the raw spectrum, data from each output of the system at different phase switch states have been integrated. In the processed spectrum, data have been averaged in each phase switch state and then differences calculated between consecutive states. These last results have been Fourier transformed.

4.2 Special Cases of Simulations: Switching Frequency and Gain Fluctuations

In the simulation, gain fluctuation is controlled in amplitude and speed, depending on the level of the noisy signals and the shape of the low-pass filters used in the 1/f generation.

Faster and slower gain-controlling signals were used, and different switching frequencies were compared in terms of the output signal spectrum.

A minimum postdetection bandwidth is required to ensure that both phase switch states are clearly distinguished at the output; therefore, several harmonics of the switching signal must pass the output filter. Commutation of the phase switches may take place in two ways: switching both branches to a fixed frequency (i.e., 4 KHz) or leaving a fixed phase in one branch and switching the other with double the frequency (8 KHz). In both cases, sky and reference signals alternate at the outputs. If a switching frequency of 8 KHz is considered, a well-defined square-wave would require at least five harmonics (40 KHz). Therefore, a simulation must be defined to check if the postdetection bandwidth is enough to fulfill the bandwidth condition. In these simulations, the transient envelope becomes quite useful because magnitude of the fundamental tone can be plotted versus

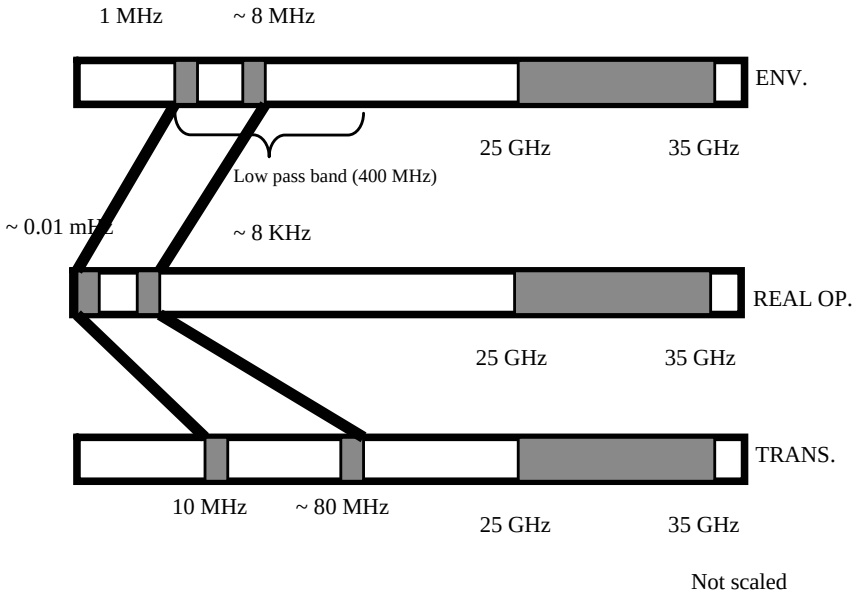

Figure 22. Examples of frequency time scales present in the envelope simulation, transient simulation, and, in the middle, real operation of the radiometer

time and superimposed with the switching signal and output signal. But here the limitations in maximum time (minimum frequency) arise, which force us to simulate not with real frequencies (KHz) but with higher frequencies (MHz). One possibility is to introduce pulsed RF in one input and check the DC output without switching. Figure 23 shows the magnitude of the fundamental tone versus time at the input of the radiometer and at the input of the detector (RF) and superimposed with the output signal (DC).

Another possibility is to apply a continuous-wave (CW) tone (e.g., in the sky input), leaving a noise source in the reference input with phase switching active. The CW tone has amplitude large enough to stand out from the noise and to show the effect clearly, but in real operation, power levels are much lower and very similar; therefore, less response time is required. Magnitude of the fundamental tone has been plotted versus time and superimposed with the switching signal and the output signal. This simulation is done for the same output and the same bandwidth but for two switching periods, the second 10 times higher, showing a clear difference in the speed of response (see Fig. 24a,b).

Using nominal input signals with realistic and complete models, including thermal noise and fluctuations, the comparison of both outputs (Fig. 25) and the comparison of successive states in one branch can be made to obtain the instantaneous and averaged *r* factor (*r* factor averaged values are 0.944 for the first case and 0.948 for the second).

The estimation of $f_{k_{nee}}$ from simulations is easy due to the possibility of performing two different analyses: one with gain fluctuations "off" and the other with gain fluctuations "on." The value of $f_{k_{nee}}$ is estimated by integrating the raw output spectrum of the second simulation as far from the DC as possible (but below the roll-off of the post-detection bandwidth) up to the frequency at which power is twice the power corresponding to the first simulation (white noise sources). In Figure 26, the raw spectrum of one output for the two cases is superimposed: only thermal noise and thermal noise plus gain noise fluctuations. The flat line represents the numerically averaged in-band thermal noise power density. The value of $f_{k_{nee}}$ is numerically estimated to be 83 MHz for this case.

If both output signals are combined with an *r* factor, taking into account the phase switch state, different knee frequencies can be obtained as a function of *r*. The operation of comparison with *r* factor correction can be done by software. The ideal situation is a continuous correction of *r* value, but depending on telemetry limitations, it could be necessary to have an averaged and refreshed estimation of the *r* factor. The values of $f_{k_{nee}}$ versus *r* factor for the difference between both channel outputs are plotted for slow switching frequency and fast gain fluctuation (see Table 1 and Fig. 27). It proves that adequate choice of *r* minimizes $f_{k_{nee}}$. Note that, as could be expected, differencing both outputs decreases $f_{k_{nee}}$ compared to differencing consecutive states in the same output. In the first case, the compared sky and ref signal flow simultaneously through the system (same gain), but in the second case, compared signals flow in consecutive moments (possibly different gain). Another result is that the minimum $f_{k_{nee}}$ corresponds to differencing both outputs with fast switching frequency

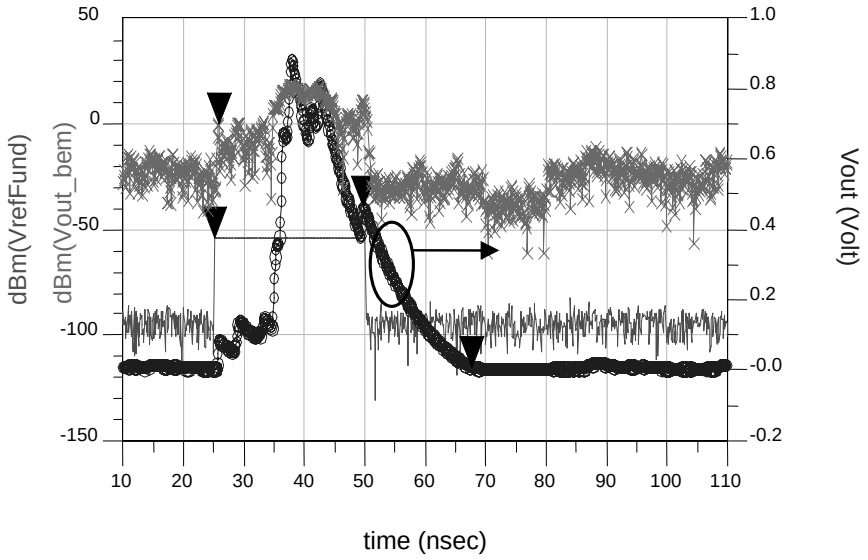

Figure 23. Magnitude of the fundamental tone at the input of the radiometer (line) and at the input of the RF detector (x) and superimposed with output signal (circles), all versus time

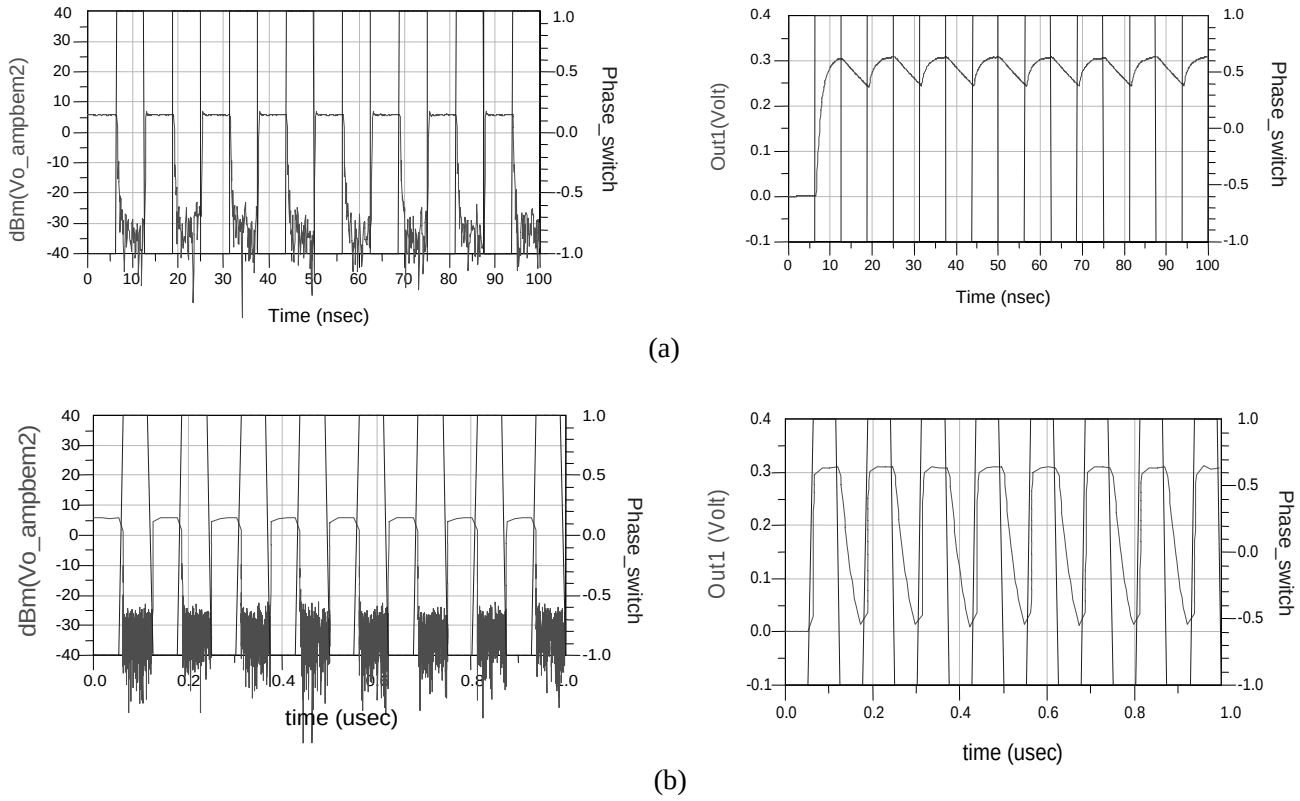

Figure 24. Magnitude of the fundamental tone at the RF output of back-end module (BEM) versus time and superimposed with switching signal (left) and corresponding output signal (right). Two switching periods: the lower (b) is 10 times higher than the upper (a) but with the same output bandwidth.

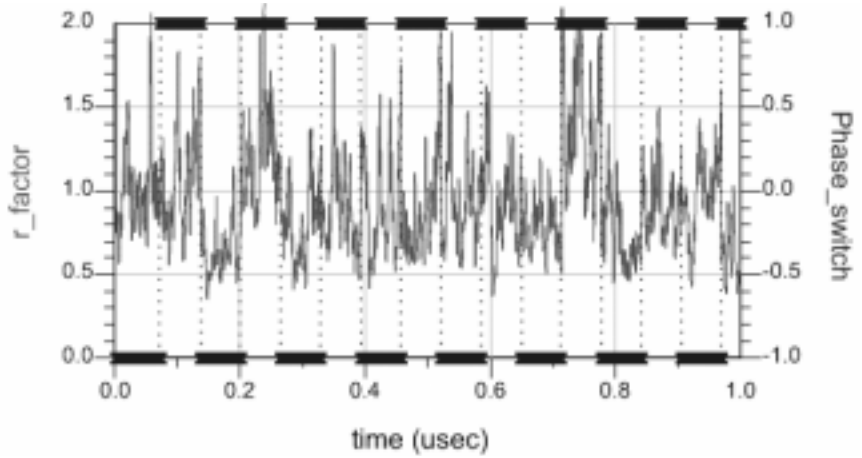

Figure 25. r factor differencing output of both branches (line) for fast fluctuations and slow switching. Average value: 0.944. Phase switch control signal is also plotted (x).

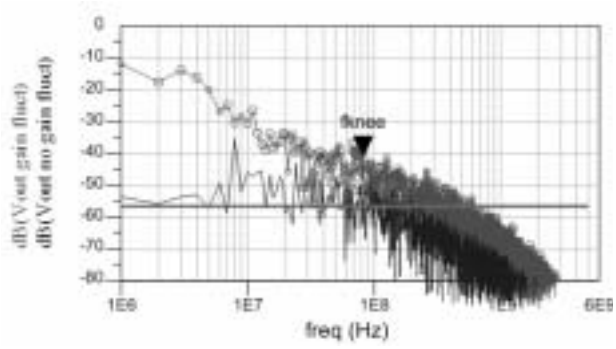

Figure 26. Raw spectrum of one output for several cases: thermal noise only and gain-noise fluctuations. Flat line: averaged in-band thermal noise power density. f_{knee} is numerically estimated to be 83 MHz.

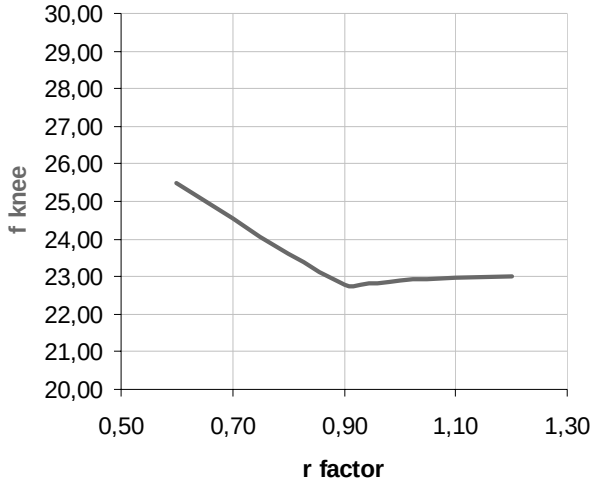

Figure 27. Differencing r factor versus f knee for fast fluctuation and slow switching

and slow gain fluctuation (in this case almost null, which means suppression of the 1/f noise). In this case, switching happens without giving the gain time to vary.

Gain-noise fluctuations have been measured and simulated for BEM alone without phase switching to adjust the levels of fluctuations, supposing a 290 K matched load at the input. Both spectra must be compared, taking into account low-frequency shift of simulations (Figs. 28, 29).

Transient envelope simulations can be used to get an estimation of the effective bandwidth (defined in equation (7)), but using an approach derived from equation (8) [12]:

$$\frac{\Delta V}{V} = \frac{1}{\sqrt{BW_{eff}\tau}}, \tag{11}$$

where ΔV is the RMS white noise spectral density at the output, τ is the integration time of the postdetection filter, and V is the output DC value. It can be demonstrated [12] that

$$BW_{eff} = 2\frac{V^2}{\Delta V^2}. \tag{12}$$

In Figure 30, data to compute equation (12) are obtained. Effective bandwidth calculated is 4.2 GHz.

4.3 Processed Spectrum

Simulated data from both outputs can be stored in a file and then loaded from a mathematical tool (such us MatLab) to process the data. Processing consists of averaging data

Table 1. Effect on f knee of differencing between outputs or with the same output delayed, for different combinations of switching speed and gain fluctuation (output bandwidth is around 400 MHz)

Gain Fluctuation (1/f Noise Filter Fcut off)	Switching Frequency	F_{knee} #1–#1 Delayed	F_{knee} #1–#2
Fast (14.9 MHz)	Fast (80 MHz)	125 (r = 0.92)	77.31 (r = 0.93)
Fast (14.9 MHz)	Slow (8 MHz)	47 (r = 0.92)	23.6 (r = 0.93)
Slow (4.6 MHz)	Fast (80 MHz)	< 1	< 1
Slow (4.6 MHz)	Slow (8 MHz)	11.6 (r = 0.92)	6.6 (r = 0.93)

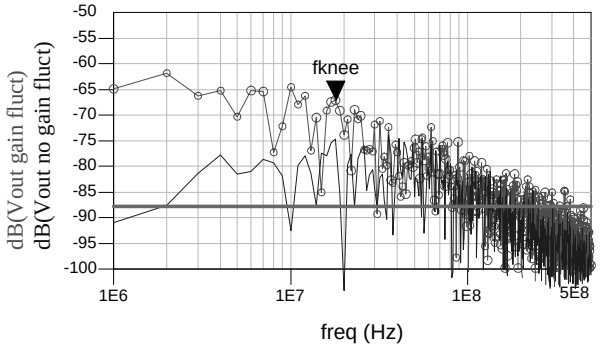

Figure 28. Simulated back-end module (BEM) output spectrum without gain-noise fluctuations and with gain-noise fluctuations included (circles). Horizontal line is the average in band white noise level.

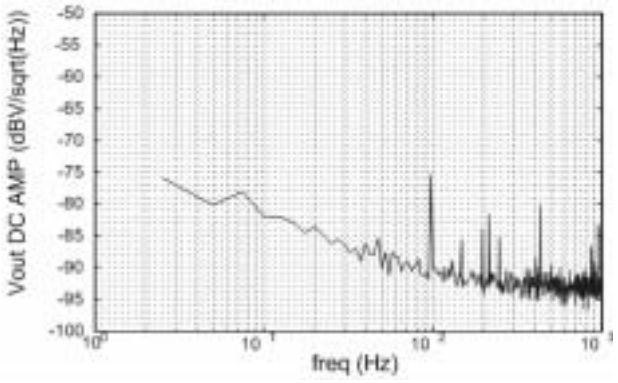

Figure 29. Measured BEM output spectrum

in each phase switch state and then differencing between consecutive states in the same output or in both outputs. If the simulated time is too short, taking into account that the number of points after averaging decreases, it may be possible to virtually build a cloned version of the signal (with an odd number of repetitions to avoid introducing false periodicities) by replicating the same waveform but

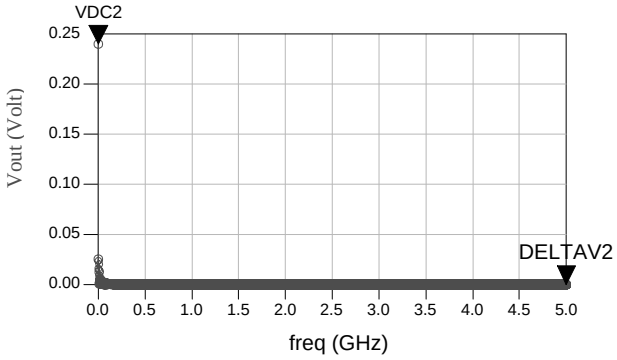

Figure 30. Estimation of the effective bandwidth using the output spectrum

mirrored in time to maintain continuity. When processing data, the time step can be multiplied to reduce frequency step and maximum frequency.

Another possibility that is beyond the scope of this article is to process data using wavelets [13] or Allan variance, which can be used as a figure of merit of system gain stability [14].

5. Conclusions

A complete set of simulation tools and procedures has been proposed and tested to emulate, on a RF-microwave software package, the behavior of a differential radiometer. In particular, they have been applied to a branch of the 30-GHz radiometer of the Planck mission. Several methods have been proposed to overcome limitations in built-in models of different system elements, spectrum coverage, and memory handling of the simulator. Further work is being done to refine the simulations by including other sources of fluctuations and errors, but the principles have been established. Figure 31 summarizes the main relationships between types of simulations and parameters of interest. Intersection of ellipses means concurrence of transient and harmonic balance in the transient envelope tool. Notice that effective bandwidth and sensitivity parameters are obtained indirectly, by the application of approximated for-

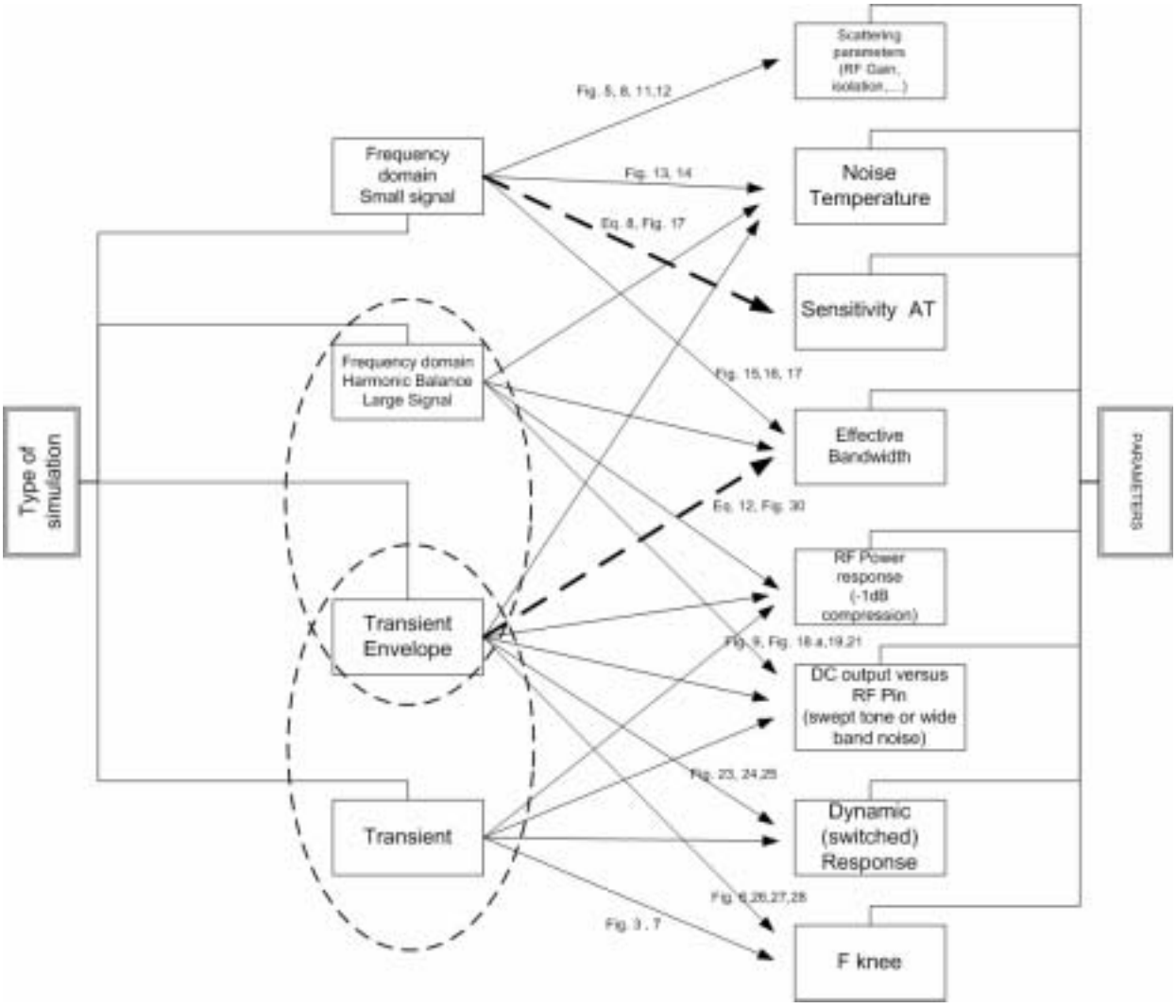

Figure 31. Diagram summarizing relationships between types of simulations and parameters. Dashed arrow means relationship by approximate equation. Indicated figures correspond to cases of such simulations.

mulas in two cases: equations (8) and (12). Figure numbers indicate corresponding simulations.

This methodology could be applied to radiometers operating in other frequency windows with other structures and even extended to other "ultra-wide-band systems."

6. Acknowledgments

This work has been financed by the Spanish Ministerio de Educación y Ciencia, through its Space National Program (references ESP2002-04141-CO3-03 and ESP2004-07067-CO3-02), and by the project "Nuevas técnicas para el análisis y diseño de divisores de frecuencia" (ref. no TIC2002-03748).

7. References

[1] ESA Astrophysics home page of Science team of Planck. http://sci.esa.int/planck

[2] Menella, A., M. Bersanelli, R. C. Butler, D. Maino, N. Mandolesi, et al. 2003. Advanced pseudo-correlation radiometers for the Planck-Lfi instrument. In *3rd ESA Workshop on Millimeter Wave Technology and Applications*, May, pp. 69-74.

[3] Portilla, J., E. Artal, and E. Martinez- Gonzalez. 2000. Analysis of the 1/f-noise effects on the Planck low-frequency instrument receivers. *Astrophysical Letters and Communications* 37:195-203.

[4] Burrage, D. M., M. A. Goodberlet, and M. L. Heron. 2002. Simulating passive microwave radiometer design using Simulink. *Simulation* 78 (1): 36-55.

[5] Yarovoy, A. 2003. Ultra wide band systems. In *Proceedings of the 33rd European Microwave Conference*, October, Munich, Germany, pp. 597-600.

[6] Advanced Design System (ADS) Documentation. http://eesof.tm.agilent.com/docs/adsdoc2001/doc.html
[7] Pascual, J. P., M. Rodríguez Gironés, M. L. De La Fuente, F. López, C. I. Lin, A. Simon, and H. L. Hartnagel. 1999. Subharmonically pumped MMIC mixer operating at 150 GHz. In *7th Symposium on Recent Advances in Microwave Technology (ISRAMT)*, December, Málaga, Spain, pp. 248-51.
[8] Artal, E., B. Aja, M. L. de la Fuente, C. Palacios, A. Mediavilla, J. P. Pascual, and J. Portilla. 2001. Low 1/F noise 30 GHz broadband amplifiers for the differential radiometers of the Planck surveyor mission. In *Proceedings of the 31st European Microwave Conference*, vol. 2, London, pp. 61-4.
[9] Jarosik, N. C. 1996. Measurements of the low-frequency-gain fluctuations of a 30GHz high-electron-mobility-transistor cryogenic amplifier. *IEEE Transactions on Microwave Theory and Techniques* MTT-44 (2): 193-7.
[10] Ulaby, F., R. More, and A. Fung. 1981. *Microwave remote sensing: Vol. 1. Microwave remote sensing fundamentals and radiometry*. Norwood, MA: Artech House.
[11] Ngoya, E., and R. Larcheveque. 1996. Envelope transient analysis: A new method for the transient and steady state analysis of microwave communication circuits and systems. *IEEE MTT Symposium Digest* 3:1365-8.
[12] Tiuri, M. E. 1964. Radio astronomy receivers. *IEEE Transactions on Antennas and Propagation* AP-12:930-8.
[13] Graps, A. 1995. An introduction to wavelets. *IEEE Computational Sciences and Engineering* 2 (2): 50-61.
[14] Risacher, C., and V. Belitsky. 2002. Low noise cryogenic if amplifiers for super heterodyne radioastronomy receivers. In *XIII International Symposium on Space Terahertz*, March, Boston.

J. P. Pascual *is assistant professor at the University of Cantabria, Santander.*

B. Aja *is researcher and PhD Student at the University of Cantabria, Santander.*

M. L. de la Fuente *is assistant professor at the University of Cantabria, Santander.*

T. Pomposo *was end-of-career student at the University of Cantabria, Santander.*

E. Artal *is professor at the University of Cantabria, Santander.*